

## Re-evaluation of heat flow data near Parkfield, CA: Evidence for a weak San Andreas Fault

Patrick M. Fulton,<sup>1</sup> Demian M. Saffer,<sup>1</sup> Robert N. Harris,<sup>2</sup> and Barbara A. Bekins<sup>3</sup>

Received 28 December 2003; revised 12 February 2004; accepted 5 March 2004; published 24 June 2004.

[1] Improved interpretations of the strength of the San Andreas Fault near Parkfield, CA based on thermal data require quantification of processes causing significant scatter and uncertainty in existing heat flow data. These effects include topographic refraction, heat advection by topographically-driven groundwater flow, and uncertainty in thermal conductivity. Here, we re-evaluate the heat flow data in this area by correcting for full 3-D terrain effects. We then investigate the potential role of groundwater flow in redistributing fault-generated heat, using numerical models of coupled heat and fluid flow for a wide range of hydrologic scenarios. We find that a large degree of the scatter in the data can be accounted for by 3-D terrain effects, and that for plausible groundwater flow scenarios frictional heat generated along a strong fault is unlikely to be redistributed by topographically-driven groundwater flow in a manner consistent with the 3-D corrected data.

**INDEX TERMS:** 8130 Tectonophysics: Heat generation and transport; 8150 Tectonophysics: Plate boundary—general (3040); 8164 Tectonophysics: Stresses—crust and lithosphere. **Citation:** Fulton, P. M., D. M. Saffer, R. N. Harris, and B. A. Bekins (2004), Re-evaluation of heat flow data near Parkfield, CA: Evidence for a weak San Andreas Fault, *Geophys. Res. Lett.*, 31, L15S15, doi:10.1029/2003GL019378.

### 1. Introduction

[2] The San Andreas Fault (SAF) has been interpreted to be anomalously weak on the basis of both mechanical and thermal data [Zoback *et al.*, 1987; Lachenbruch and Sass, 1980 (herein referred to as L&S, 1980)]. Maximum stress orientations inferred from borehole breakouts and earthquake focal mechanisms have been interpreted as evidence that the fault is weak (i.e., it supports shear stresses <20 MPa averaged over the seismogenic crust, ~5 times less than expected for hydrostatic pore pressure and laboratory-derived friction laws) [e.g., Zoback *et al.*, 1987]. However, interpretation of the stress orientation data is controversial; the data have been variously interpreted to indicate a weak fault in a strong crust [e.g., Townend and Zoback, 2004], a weak fault in a weak crust [Hardebeck and Hauksson, 1999], and a strong fault in a strong crust [Scholz, 2000]. The lack of a detectable heat flow anomaly across the fault—as is predicted by conductive models for frictional heating along a strong fault—has also been interpreted as

indicating a weak fault (L&S, 1980). However, considerable uncertainty remains regarding the effects of real-world variants from the no-topography, pure-conduction model on observed heat flow, and there is a large degree of scatter in the Coast Range heat flow surrounding the SAF which is to date unexplained [e.g., Sass *et al.*, 1997; L&S, 1980]. It has been argued that a strong SAF may actually generate frictional heat, but hydrogeologic effects and scatter in the heat flow data mask the expected thermal anomaly [Scholz, 2000].

[3] Processes that can potentially have significant effects on surficial determinations of heat flow include heat advection by thermally-driven convection or topographically-driven groundwater flow, topographic refraction, refraction caused by variable thermal conductivity, uncertainty in thermal conductivity, uplift and erosion, and significant variability in heat production. Saffer *et al.* [2003] evaluated the effects of topographically-driven groundwater flow on heat flow near the SAF for a suite of hydrogeologic and fault strength scenarios. They were able to rule out frictional heating along a strong SAF in the Mojave Desert, but the results were inconclusive at Parkfield due to the large degree of scatter in the data, uncertainty in the degree of 3-D terrain effects not accounted for in the present heat flow dataset, and incomplete correction for topography in their 2-D models.

[4] Here, we re-examine the heat flow data surrounding the SAFOD site near Parkfield (Figure 1) and re-evaluate the possibility that a frictional heat source from a strong SAF may be obscured by topographically-driven groundwater flow. First, we re-correct the raw temperature data for full 3-D terrain effects. We then compare the 3-D corrected data to simulated heat flow from numerical models that couple groundwater flow and heat transport. The models incorporate a range of hydrologic scenarios along three cross-sections perpendicular to the fault near the SAFOD site (Figure 1).

### 2. Methods

#### 2.1. 3-D Terrain Corrections

[5] Terrain effects are disturbances to the background temperature regime within the solid Earth caused by 3-D heat transfer due to topography, variable solar insolation, and variations in thermal and radioactive properties of the Earth's surface [Blackwell *et al.*, 1980]. Most of the heat flow measurements we use in this study have previously been published with limited 2-D terrain corrections, which use exact solutions for simple geometric shapes that approximate the true topographic surface along a transect perpendicular to the general strike of topography. These models assume a constant surface temperature or one that varies linearly with elevation, and do not take into account

<sup>1</sup>Department of Geology and Geophysics, University of Wyoming, USA.

<sup>2</sup>Department of Geology and Geophysics, University of Utah, USA.

<sup>3</sup>U.S. Geological Survey, Menlo Park, California, USA.

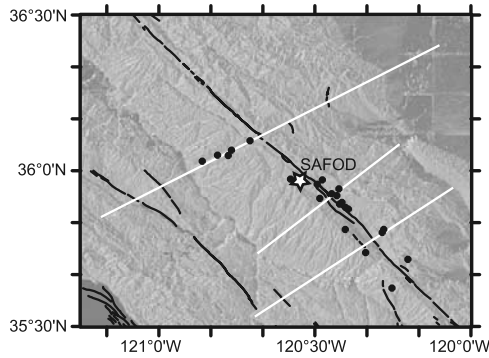


**Figure 1.** Shaded relief map of Parkfield area showing model transects (white lines), locations of existing heat flow measurements (black circles), the SAFOD site (star), and mapped faults in the region (black lines).

effects of variable solar insolation that may alter the surface temperature around a borehole. *Blackwell et al.* [1980] note that in cases where there is appreciable topographic variation, and especially if the topography is dominantly of one sign (i.e., on a hilltop or in a canyon), these solutions are unsatisfactory for boreholes with depths  $<300$  m.

[6] We correct the raw temperature data using a more complete terrain correction, which takes into account 3-D topography and solar insolation effects [*Blackwell et al.*, 1980]. We calculate the surface temperature field as a function of variations in elevation coupled with a lapse rate and in solar insolation due to the angle and azimuth of terrain slopes [e.g., *Powell*, 1997]. Estimated surface temperatures are fit with a Fourier series and upward continued ( $z$  positive down) [*Blackwell et al.*, 1980, equation 7], to find the subsurface temperature field free of terrain effects. We have applied the correction for 22 boreholes near Parkfield, CA, and report the least squares fit corrected gradient over a depth interval of known thermal conductivity (Table 1). Heat flow ( $q$ ) is calculated by:

$$q = -\lambda_{\text{avg}} dT/dz \quad (1)$$

where  $\lambda_{\text{avg}}$  is the mean thermal conductivity over the depth interval, and  $dT/dz$  is the corrected thermal gradient over the same interval.

[7] The corrected gradient for each borehole is well constrained; however, thermal conductivity values are subject to large uncertainties, mainly due to undersampling. For some boreholes, thermal conductivity data are not available and values are based on formation averages [e.g., *Sass et al.*, 1997]. We define error bars for the heat flow data (Table 1, Figure 3) as the product of standard deviation of thermal conductivity ( $\sigma_{\Lambda}$ ) and the corrected gradient:

$$q = -\lambda_{\text{avg}} dT/dz \pm \sigma_{\Lambda} dT/dz \quad (2)$$

## 2.2. Topographically-Driven Groundwater Flow

[8] To evaluate the possibility that the SAF generates frictional heat, but that the thermal signal is masked by the effects of groundwater flow, we simulate 2-D coupled heat and fluid flow along three transects (Figure 1) for a series of groundwater flow and fault strength scenarios. The models

we use to simulate heat flow are an adaptation of the pure-conduction models of L&S (1980) in which we include a topographic surface and allow for fluid flow [e.g., *Saffer et al.*, 2003]. We solve the steady-state coupled fluid and heat flow equations with the finite-element code, SUTRA [*Voss*, 1984]. The side boundaries of each cross-sectional model coincide with regional groundwater divides and are set as no-flow boundaries for fluid and heat. We assign the water table at the top surface, defined by the topography along each cross-section, and specify the surface temperature with an atmospheric lapse rate of 6.9 K/km. We assign a basal heat flux of 78 mW/m<sup>2</sup> along the bottom boundary, equivalent to the regional average for the Central Coast Ranges (L&S, 1980).

[9] To simulate a strong fault, we include a line heat source at the fault that increases linearly with depth by 8.85 mW/m<sup>2</sup> per km (consistent with a shear-stress gradient of 9 MPa/km and a long-term average slip rate of 3.1 cm yr<sup>-1</sup>). To simulate a weak fault we include a heat source increasing linearly with depth by 1.97 mW/m<sup>2</sup> per km (reflecting a shear-stress gradient of 2 MPa/km). We evaluate a range of groundwater flow scenarios by defining permeability ( $k$ ) within the model domain. We consider a suite of scenarios in which  $k$  is homogeneous, ranging from 10<sup>-17</sup> to 10<sup>-15</sup> m<sup>2</sup>, and two cases in which  $k$  decreases exponentially with depth [e.g., *Ingebritsen and Manning*, 1999; *Williams and Narisimhan*, 1989]:

$$f(\text{depth})_{\text{high}} : \log(k_{xx}) = -14 - 3.2 \log(z); k_{zz} = k_{xx}/10 \quad (3)$$

$$f(\text{depth})_{\text{low}} : \log(k_{xx}) = -15 - 3.2 \log(z); k_{zz} = k_{xx}/10 \quad (4)$$

**Table 1.** 3-D Corrected Heat Flow Data Near Parkfield, CA

Well ID	Ref <sup>a</sup>	$\lambda\sigma_{\Lambda}$ [W m <sup>-1</sup> K <sup>-1</sup> ]	# $\lambda$	$z_1-z_2$ [m]	$dT/dz$ [°C km <sup>-1</sup> ]	$q \pm \sigma_q$ [mW m <sup>-2</sup> ]
EADE	a	2.77 ± 0.20	0	152–258	30.19	84 ± 6
EDE2	a	2.52 ± 0.22	9	177–277	32.68	82 ± 7
FROL	a	2.05 ± 0.20	24	152–277	35.31	72 ± 7
PDCH	a	1.80 ± 0.20	0	61–182	47.41	85 ± 9
PDCH_deep	a	2.00 ± 0.75	0	232–305	34.08	68 ± 26
PDCH_avg	a					77 ± 17
PDDL	a	1.92 ± 0.14	0	61–304	37.80	73 ± 5
PDHF	a	2.77 ± 0.20	0	91–305	33.01	91 ± 7
PDJC	a	3.29 ± 0.20	4	119–131	25.30	83 ± 5
PDJC_deep	a	2.84 ± 0.22	9	162–179	27.76	79 ± 6
PDJC_avg	a					81 ± 4
PDL2	a	1.92 ± 0.14	18	91–207	35.44	68 ± 5
PDRH	a	2.04 ± 0.10	5	183–228	31.12	63 ± 3
PDSC	a	2.77 ± 0.20	0	61–122	23.60	65 ± 5
PDSM	a	1.50 ± 0.10	4	80–182	47.79	72 ± 5
PDSM_deep	a	3.20 ± 0.20	2	182–298	28.27	90 ± 6
PDSM_avg	a					81 ± 0
PDWC	a	1.80 ± 0.20	0	187–302	38.92	70 ± 8
PHF2	a	2.77 ± 0.20	0	122–305	30.77	85 ± 6
PPC2	a	1.92 ± 0.14	0	122–203	39.42	76 ± 6
PR1	b	1.07 ± 0.13	15	182.9–219.6	73.73	79 ± 9
PR2	b	1.07 ± 0.13	0	70.1–128.1	68.29	73 ± 9
PR3	b	1.07 ± 0.13	0	60–120	87.93	94 ± 11
PR4	b	1.60 ± 0.02	3	265–280	52.41	84 ± 1
PSC2	a	2.55 ± 0.20	4	152–303	30.79	79 ± 6
USL	b	1.07 ± 0.13	0	400–475	78.18	84 ± 10
VARN	a	2.20 ± 0.20	14	63–226	36.87	81 ± 7
VARN_deep	a	2.50 ± 0.20	11	226–304	29.10	73 ± 6
VARN_avg	a					77 ± 2
VARP	a	2.03 ± 0.09	7	1219–1555	35.16	71 ± 3

<sup>a</sup>a, L&S (1980); b, *Sass et al.* [1997].

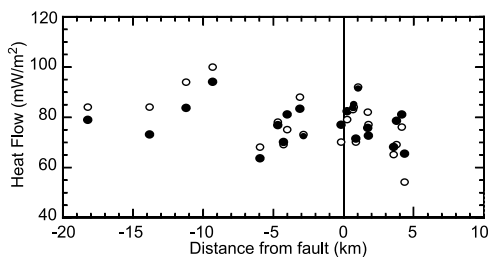


**Figure 2.** 3-D corrected heat flow data (solid circles) and previously published data (open symbols) vs. distance from the SAF.

We report simulated heat flow values computed from the modeled steady-state temperature field at the depth interval between 100–200 m, and corrected for topographic effects along the model transect using a 2-D solid-angle method [Birch, 1950].

### 3. Results and Discussion

#### 3.1. Terrain Correction

[10] The degree of scatter in heat flow data is greatly reduced by applying the 3-D terrain correction (Figure 2). Standard deviation is reduced by 26% from the previously published data. The largest corrections generally occur for boreholes with published heat flow values that deviated significantly from the regional average. Published values greater than 86 mW/m<sup>2</sup> are reduced by up to 11 mW/m<sup>2</sup>, and 5.6 mW/m<sup>2</sup> on average; published values less than

70 mW/m<sup>2</sup> are increased by as much as 11 mW/m<sup>2</sup>, and 4.1 mW/m<sup>2</sup> on average.

[11] Similarly, correction of simulated heat flow for 2-D model topography—not fully accounted for in previous studies—significantly reduces the scatter in these values, allowing the thermal signature from heating along a strong vs. a weak SAF to be more distinguishable. Importantly, the large degree of scatter in both the published dataset and their simulated heat flow led *Saffer et al.* [2003] to conclude that observed heat flow could be consistent with either a strong or weak SAF near Parkfield. With the 3-D corrections, there are no indications of a statistically significant pattern of higher heat flow near the fault as expected if it were strong. Additional effects on heat flow due to uplift and erosion, thermally-driven convection, or variability in thermal conductivity and heat production are considered small or unlikely causes for masking a heat-flow anomaly generated by a strong SAF [e.g., *Williams and Narisimhan*, 1989; *Lachenbruch and Sass*, 1992].

#### 3.2. Fault Strength and the Extent of Groundwater Flow

[12] To evaluate plausible fault strength scenarios, we visually compare simulated heat flow to the 3-D corrected data along the model profiles (Figure 3) and compare the observed and modeled heat flow difference near and far from the SAF (Figure 4a). We then identify plausible groundwater flow scenarios by comparing the variability in modeled heat flow with that observed.

[13] For conduction-dominated heat transport ( $k < 10^{-16} \text{ m}^2$ ), strong fault models predict a fault-centered heat flow anomaly of peak magnitude 31–37 mW/m<sup>2</sup> (Figure 3a), which overpredicts heat flow within 9 km of the fault. If the actual regional heat flow is lower than the

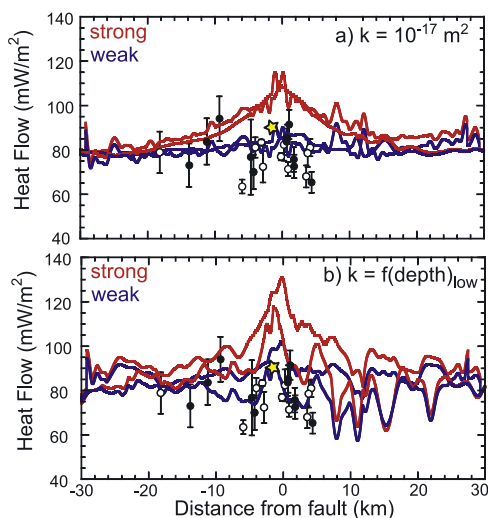


**Figure 3.** Comparison of heat flow data and simulated heat flow for plausible groundwater flow conditions from all three transects, projected along-strike and registered to the fault at  $x = 0$ , for (a)  $k = 10^{-17} \text{ m}^2$ , and (b)  $k = f(\text{depth})_{\text{low}}$ . Colored lines show simulated heat flow for heating along a strong (red) and weak (blue) SAF; the two lines for each scenario indicate the range of simulated heat flow for the three transects. We differentiate between boreholes that have thermal conductivity measurements (open) and those that use formation averages (solid). The star (yellow) represents the heat flow value for the SAFOD pilot hole [Williams et al., 2004].

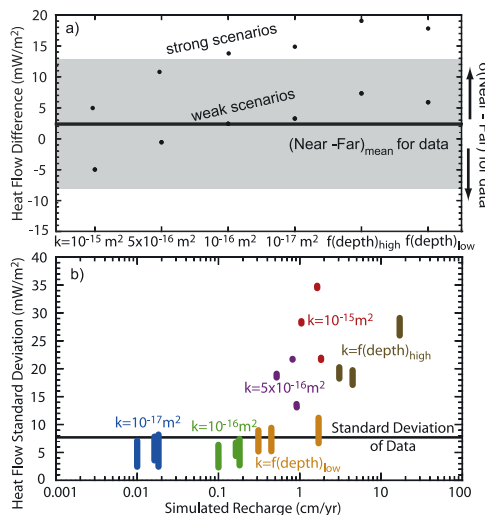


**Figure 4.** (a). Comparison of the near-fault heat flow anomaly, defined as the difference between heat flow near (<3 km) and far (>3 km) from the fault, predicted by each simulation (individual points) to that observed (the black line represents the mean and the grey box the standard deviation in the observed difference.) (b). Variability in observed heat flow (black line) compared with that predicted by each groundwater flow scenario (colored bars) as a function of the mean recharge required.

basal heat flux used in our models (78 mW/m<sup>2</sup>), it would be possible to fit some near-fault data with a strong fault model. However, in order to fit the data within 9 km of the fault in this manner, a downward static shift of  $\sim 30$  mW/m<sup>2</sup> would be needed, implying a regional heat flow of  $\sim 48$  mW/m<sup>2</sup>. This is an unrealistic value for the regional average; L&S (1980) report only one value  $< 50$  mW/m<sup>2</sup> within 200 km of the Parkfield area. Furthermore, this static shift is inconsistent with heat flow values away from the fault.

[14] In contrast, models that incorporate heating along a weak fault predict a small near-fault anomaly, and fit the data better both near and away from the fault—including the deep heat flow determination from the SAFOD site [Williams *et al.*, 2004] (Figure 3a). Simulated heat flow for frictional heating along a strong fault is consistent with the data only for models that allow significant near-surface groundwater flow ( $k > 10^{-16}$  m<sup>2</sup> and  $f(\text{depth})_{\text{high}}$ ), whereas simulations that incorporate frictional heating along a weak fault are generally consistent with the data for all groundwater flow scenarios we investigated (e.g., Figure 3).

[15] For strong fault scenarios, models predict a systematic difference between heat flow near and away from the SAF for many of the groundwater flow scenarios (Figure 4a). The data indicate a difference of  $2.3 \pm 10.5$  mW/m<sup>2</sup>. The large uncertainty results from remaining scatter even in the 3-D corrected data, and, in many cases, large uncertainty in thermal conductivity. Based on the observed difference between heat flow near and away from the SAF, heat generation on a weak fault is consistently allowable, whereas heating along a strong fault is consistent only for the highest permeability models ( $k > 5 \times 10^{-16}$  m<sup>2</sup>) in which the surface expression of frictional heating is no longer distinguishable. These higher permeabilities allow for significant near-surface groundwater flow which results in a high degree of variability in simulated heat flow.

[16] To identify plausible groundwater flow scenarios, we compare the variability in heat flow observed in the 3-D corrected data to modeled heat flow over the same spatial window ( $-18.2$  to  $4.3$  km from the fault) (Figure 4b). Simulations with permeabilities  $> 10^{-16}$  m<sup>2</sup> in the upper km drive recharge rates  $> \sim 1$  cm/yr, resulting in significantly larger variability in the heat flow than observed (Figure 4b). On this basis, and based upon the lack of a pronounced relationship between observed heat flow and elevation [Saffer *et al.*, 2003], we consider scenarios characterized by such high groundwater fluxes to be unreasonable. Williams *et al.* [2004] note that the depth extent of seismicity corresponds to a temperature of  $\sim 350^\circ\text{C}$  projected downward using surface heat flow, further suggesting that the heat flow measurements are not highly disturbed by advection.

#### 4. Conclusions

[17] Much of the scatter in the previously published heat flow data near Parkfield can be accounted for by 3-D terrain effects. The 3-D terrain corrected data show no discernable fault-centered thermal anomaly within the uncertainty of thermal conductivity values, and are most consistent with a

small degree of heat generation along the SAF. Simulated heat flow for all groundwater flow scenarios that incorporate a weak fault is generally consistent with the data. Models that incorporate frictional heating along a strong fault are only consistent with the data for high-permeability scenarios that allow significant near-surface groundwater flow. We rule out the plausibility of these advection-dominated scenarios because they predict a high degree of variability in the heat flow, which is not observed. Thus, for plausible groundwater flow scenarios, simulated heat flow is most consistent with heat generation along a weak SAF. This corresponds well with recent analyses of stress data which imply that fault strength is “extremely low” in Central California [Townend and Zoback, 2004]. We conclude that frictional heat generated along a strong fault is unlikely to be redistributed by topographically-driven groundwater flow in a manner that would be consistent with the data when fully corrected for terrain effects.

[18] **Acknowledgment.** This work was supported by NSF grants EAR 0125189 to Saffer and EAR 0087577 to Harris.

#### References

- Birch, F. (1950), Flow of heat in the Front Range, Colorado, *Geol. Soc. Am. Bull.*, *61*, 567–630.
- Blackwell, D. D., J. L. Steele, and C. A. Brott (1980), The terrain effect on terrestrial heat flow, *J. Geophys. Res.*, *89*, 4757–4772.
- Hardebeck, J. L., and E. Hauksson (1999), Role of fluids in faulting inferred from stress field signatures, *Science*, *285*, 236–239.
- Ingebritsen, S. E., and C. E. Manning (1999), Geological implications of a permeability-depth curve for the continental crust, *Geology*, *27*, 1107–1110.
- Lachenbruch, A. H., and J. H. Sass (1980), Heat flow and energetics of the San Andreas fault zone, *J. Geophys. Res.*, *85*, 6185–6222.
- Lachenbruch, A. H., and J. H. Sass (1992), Heat flow from Cajon Pass, fault strength, and tectonic implications, *J. Geophys. Res.*, *97*, 4995–5015.
- Powell, W. G. (1997), Thermal state of the lithosphere in the Colorado Plateau - Basin and Range transition zone, Utah, Ph.D. Dissertation, Salt Lake City, Univ. of Utah.
- Saffer, D. M., B. A. Bekins, and S. Hickman (2003), Topographically driven groundwater flow and the San Andreas heat flow paradox revisited, *J. Geophys. Res.*, *108*(B5), 2274, doi:10.1029/2002JB001849.
- Sass, J. H., et al. (1997), Thermal regime of the San Andreas fault near Parkfield, California, *J. Geophys. Res.*, *102*(B12), 27,575–27,585.
- Scholz, C. H. (2000), Evidence for a strong San Andreas fault, *Geology*, *28*, 163–166.
- Townend, J., and M. D. Zoback (2004), Regional tectonic stress near the San Andreas fault in central and southern California, *Geophys. Res. Lett.*, *31*, L15S11, doi:10.1029/2003GL018918.
- Voss, C. I. (1984), A finite-element simulation model for saturated-unsaturated fluid density-dependent groundwater flow with energy transport or chemically reactive single-species solute transport, USGS, *Water Resources Investigations Report*, 84–4369.
- Williams, C. F., and T. N. Narisimhan (1989), Hydrogeologic constraints on heat flow along the San Andreas fault: A testing of hypotheses, *Earth Planet. Sci. Lett.*, *92*, 131–143.
- Williams, C. F., F. V. Grubb, and S. P. Galanis Jr. (2004), Heat flow in the SAFOD pilot hole and implications for the strength of the San Andreas Fault, *Geophys. Res. Lett.*, *31*, L15S14, doi:10.1029/2003GL019352.
- Zoback, M. D., et al. (1987), New evidence on the state of stress of the San Andreas Fault, *Science*, *238*, 1105–1111.

- B. A. Bekins, U.S. Geological Survey, Menlo Park, California, USA.  
 P. M. Fulton and D. M. Saffer, Department of Geology and Geophysics, University of Wyoming, USA. (pfulton@uwyo.edu)  
 R. N. Harris, Department of Geology and Geophysics, University of Utah, USA.